PNAS RESEARCH ARTICLE | DEVELOPMENTAL BIOLOGY

Maintenance of hematopoietic stem cell niche homeostasis requires gap junction–mediated calcium signaling

Kevin Y. L. Ho[a], Kevin An[a,1], Rosalyn L. Carr[a,b,c,1], Alexandra D. Dvoskin[a,1], Annie Y. J. Ou[a,d,1], Wayne Vogl[a], and Guy Tanentzapf[a,2]

Edited by Utpal Banerjee, University of California, Los Angeles, CA; received February 22, 2023; accepted September 11, 2023

Regulation of stem cells requires coordination of the cells that make up the stem cell niche. Here, we describe a mechanism that allows communication between niche cells to coordinate their activity and shape the signaling environment surrounding resident stem cells. Using the *Drosophila* hematopoietic organ, the lymph gland, we show that cells of the hematopoietic niche, the posterior signaling center (PSC), communicate using gap junctions (GJs) and form a signaling network. This network allows PSC cells to exchange Ca^{2+} signals repetitively which regulate the hematopoietic niche. Disruption of Ca^{2+} signaling in the PSC or the GJ-mediated network connecting niche cells causes dysregulation of the PSC and blood progenitor differentiation. Analysis of PSC-derived cell signaling shows that the Hedgehog pathway acts downstream of GJ-mediated Ca^{2+} signaling to modulate the niche microenvironment. These data show that GJ-mediated communication between hematopoietic niche cells maintains their homeostasis and consequently controls blood progenitor behavior.

Drosophila | hematopoiesis | stem cell niche | calcium signaling | gap junctions

Significance

The local microenvironment of stem cells, known as the stem cell niche, plays a central role in regulating the behavior of stem cells. An accumulating body of knowledge suggests that stem cell niches exhibit a great deal of plasticity which impacts stem cell homeostasis. It is imperative that changes in the microenvironment are coordinated both temporally and spatially; otherwise, the stem cells within the niche may be exposed to wrong cues which would cause dysregulation. Our manuscript describes a mechanism that coordinates the function of niche cells to ensure stem cell homeostasis. We believe that this mechanism is conserved in many stem cell niches, meaning that our results will have important wide-ranging implications.

The local microenvironment of the stem cell niche plays a central role in regulating the behavior of stem cells at the population level (1–3). There is an accumulating body of knowledge that shows that stem cell niches can exhibit a great deal of plasticity both functionally and morphologically and that this impacts stem cell homeostasis (2–4). The ability of the niche to change and evolve over time is particularly important when there is a requirement to modulate stem or progenitor cell homeostasis, for example, in response to injury, during aging, or in response to environmental stressors and stimuli (4–7). It is imperative that changes in the microenvironment are precisely coordinated both temporally and spatially; otherwise, the stem or progenitor cells that reside within the niche may be exposed to the wrong cues which would lead to dysregulation (4, 5, 8, 9). For this reason, the question of how stem cell niches act in a coordinated fashion is important for elucidating the mechanisms that ensure tissue and organ homeostasis.

The *Drosophila* hematopoietic organ, the lymph gland (LG), contains a distinct group of cells known as the PSC that control the behavior of their neighboring blood progenitors (9–12). The PSC offers a powerful, genetically tractable model system for studying stem cell niches (10). It is composed of about 35 to 50 cells that are specified during embryogenesis and maintain their distinct identity within the LG for the rest of larval life (10, 13). The PSC is well defined and can be distinguished both morphologically and molecularly. It is prominently located as a cluster on the most posterior part of the primary lobe of the LG abutting the dorsal vessel tube (10). Several molecular markers specifically label the PSC within the LG, including the homeobox protein Antennapedia (Antp), the Early B-cell Factor transcription factor Collier, and the signaling molecule Hedgehog (Hh) (12, 14–17). The primary function of the PSC is thought to be as a source of signaling molecules that act on the blood progenitors (12, 15, 17). For example, the PSC is the source of multiple secreted ligands such as Hh (15), Dpp/BMP (18), and Wingless (Wg) (19) that act on the progenitors to initiate downstream signals that promote progenitor maintenance and regulate differentiation.

The PSC itself is the subject of homeostatic regulation (20). First, the maintenance of PSC identity is an active process that requires ongoing expression of Collier (12). Second, Dpp/BMP and Wg signals actively regulate the size of the PSC, in opposite directions (18). Specifically, Dpp/BMP plays an inhibitory role in PSC size, while Wg positively regulates PSC size (18). Third, the size and morphology of the PSC are regulated by the ligand Slit, secreted from the dorsal vessel, which activates the Robo1/2 receptors in the PSC (21). Robo activation promotes DE-Cadherin expression to maintain the clustering of PSC cells and suppresses proliferation by a Dpp-mediated reduction in dMyc expression (21). Fourth, systemic nutritional signals act through insulin signaling to control PSC size (22). Specifically, the level of activity of insulin signaling in the LG directly correlates with PSC proliferation (20, 22–25). Finally, modulation

Author affiliations: [a]Department of Cellular and Physiological Sciences, University of British Columbia, Vancouver, BC V6T 1Z3, Canada; [b]School of Biomedical Engineering, University of British Columbia, Vancouver, BC V6T 1Z3, Canada; [c]British Columbia Children's Hospital Research Institute, British Columbia Children's Hospital, Vancouver, BC V5Z 4H4, Canada; and [d]School of Kinesiology, University of British Columbia, Vancouver, BC V6T 1Z1, Canada

Author contributions: K.Y.L.H. and G.T. designed research; K.Y.L.H., K.A., A.D.D., A.Y.J.O., and W.V. performed research; K.Y.L.H. and R.L.C. analyzed data; and K.Y.L.H. and G.T. wrote the paper.

The authors declare no competing interest.

This article is a PNAS Direct Submission.

[1]K.A., R.L.C., A.D.D., and A.Y.J.O. contributed equally to this work.

[2]To whom correspondence may be addressed. Email: tanentz@mail.ubc.ca.

This article contains supporting information online at https://www.pnas.org/lookup/suppl/doi:10.1073/pnas.2303018120/-/DCSupplemental.

Published October 30, 2023.

of septate junctions within the PSC affects niche homeostasis and regulates communication between the niche and blood progenitors (26). The presence of septate junctions in the PSC sets up a permeability barrier that controls the movement of Wg and Dpp/BMP ligands between the PSC and blood progenitors to regulate PSC size and blood cell differentiation (26). Overall, the emerging picture is that there are multiple cues, both systemic and local, that function to regulate PSC homeostasis. Thus, the complex signaling environment that controls PSC homeostasis presents a challenge: How to coordinate multiple, overlapping, and often opposing cues?

Gap junctions (GJs) can provide a mechanism to ensure the coordination of cell signaling across large complex organs like the LG (13, 27, 28). GJs form channels between cells that allow the transport of nutrients, signaling molecules, and small metabolites (29–32). Fly GJs are composed of innexins, which are functionally homologous to the vertebrate connexin protein family (31, 33, 34). GJs form when individual innexin subunits oligomerize to form a hemichannel on the plasma membrane (29, 34). A functional GJ is made when hemichannels on two adjacent cell surfaces dock with each other (29). The resulting GJ allows the passage of ions and small molecules between the two cells (29). In the LG, GJs connect the blood progenitors which allows them to communicate with one another directly and coordinate their behavior across large distances (13). In particular, GJs equilibrate Ca^{2+} signals between blood progenitors, which regulates their maintenance and differentiation (13). This raised the possibility that other cell types in the LG also utilize GJs to achieve functional coordination, and in the context of the PSC, this could be a key regulator in maintaining tissue homeostasis. Here, we have investigated the role of Ca^{2+} signaling and GJs in PSC niche homeostasis. We showed that GJs and Ca^{2+} signaling in the PSC play an important role in modulating both niche size and niche-derived homeostatic signals. We dissected the mechanisms that control the PSC upstream and downstream of Ca^{2+} signals as well as identified the source of Ca^{2+} in the PSC and various Ca^{2+} effectors that are downstream of the Ca^{2+} signaling network. These results suggested that homeostasis of the PSC is dependent on the ability of individual niche cells, that are exposed to the complex signaling environment of the LG, to communicate with each other through GJs on an ongoing basis.

Results

Cytosolic Ca^{2+} Levels Regulate PSC Homeostasis. Ca^{2+} signaling is an important regulator of blood progenitor homeostasis (13, 35). To determine whether Ca^{2+} plays such a role in the stem cell niche, different transgenes were expressed in the PSC, using the *collier*-Gal4 driver (12), to modulate Ca^{2+} levels and signals (Fig. 1 *A*-*B*). To elevate the cytosolic levels of Ca^{2+} in the PSC, the expression of the Ca^{2+} pump SERCA, which transports Ca^{2+} from the cytosol into the endoplasmic reticulum (ER), was knocked down using RNAi (13, 36). Three different approaches were used to lower cytosolic levels of Ca^{2+} in the PSC: 1. by expressing parvalbumin (PV), a vertebrate-specific Ca^{2+} binding protein that negatively regulates Ca^{2+} level (37, 38), 2. by RNAi-mediated knockdown of the Inositol 1,4,5-trisphosphate receptor (IP3R) (13, 36), a ligand-gated Ca^{2+} channel in the ER membrane that mobilizes ER stores of Ca^{2+}, and 3. by RNAi-mediated knockdown of the ryanodine receptor (RyR), a large-conductance channel that mediates release of Ca^{2+} from internal ER stores (39). In addition to lowering or increasing the total levels of Ca^{2+}, downstream Ca^{2+}-mediated signaling was lowered in the PSC. In particular, RNAi-mediated knockdown was used to reduce the levels of the Ca^{2+} effectors Ca^{2+}- and calmodulin-dependent protein KinaseII (CaMKII), Calcineurin A, and Calcineurin B (40). Niche homeostasis was assessed by determining the average number of PSC cells per lobe as a measure of niche size (Fig. 1 *A* and *B*). The results of this analysis showed that increasing the cytosolic levels of Ca^{2+} by knockdown of SERCA resulted in a substantial reduction in PSC size and an increase in the size of the PSC nuclei (Fig. 1 *A* and *B*). In comparison, decreasing the cytosolic levels of Ca^{2+} by expression of PV, knockdown of IP3R, or knockdown of RyR resulted in a substantially enlarged PSC (Fig. 1 *A* and *B*). Similarly, knockdown of CaMKII, Calcineurin A, or Calcineurin B also resulted in a large increase in the size of the PSC niche (Fig. 1 *A* and *B*). Finally, we assessed the role of mitochondrial Ca^{2+} uniporter (MCU), which mediates mitochondrial Ca^{2+} uptake (41, 42), in the PSC. We found that knockdown of MCU only induced a slight increase in PSC size (Fig. 1*B*). This suggests mitochondrial Ca^{2+} dynamics are not a major regulator of PSC homeostasis. Since the PSC regulates the blood progenitors (10), we investigated whether dysregulation of Ca^{2+}-mediated signaling impacted blood cell differentiation. Staining for the different blood cell markers (*Materials and Methods*) showed a significant decrease in the blood progenitor population and a substantial increase in the number of plasmatocytes but not crystal cells upon depletion of Ca^{2+} in the PSC using the expression of PV or knockdown of IP3R using RNAi (*SI Appendix*, Fig. S1 *A–C* and *E–G*). Overall, these results demonstrated that modulating Ca^{2+} levels and signaling in the PSC affects niche homeostasis and subsequently impacts blood cell differentiation.

Analysis of Ca^{2+} Signaling Dynamics and Activity in the PSC Niche. Since Ca^{2+}-mediated signaling controls niche homeostasis, we sought to visualize Ca^{2+} signaling dynamics and activity in the PSC niche. To this end, we expressed the genetically encoded Ca^{2+} indicator GCaMP6f or the sustained downstream Ca^{2+} signaling reporter CaLexA (44) in the PSC, using the driver *collier*-Gal4, and performed live imaging of intact ex vivo cultured LGs (*SI Appendix*, Fig. S2 *B* and *C*) (13). Robust Ca^{2+} signaling activity was observed in the PSC expressing GCaMP6f (Fig. 1 *C* and *D* and Movie S1), and persistent Ca^{2+} signaling activity was seen in the PSC expressing CaLexA (*SI Appendix*, Fig. S2*A*). Next, live imaging videos were analyzed to measure changes in the intensity of GCaMP signals in individual PSC cells (Fig. 1 *C–C″*). This analysis showed extensive Ca^{2+} oscillation activity and multiple Ca^{2+} spikes were generated, ranging in number from 1 to 16 spikes every 10 min (Fig. 1*D*). Quantitative analysis of the Ca^{2+} oscillations demonstrated that the oscillatory activity was stochastic. In particular, it has been shown that in many cell types exhibiting Ca^{2+} oscillations, the timing of spikes is random due to a large stochastic component in the interval between spikes (Fig. 1*E*) (43, 45). This stochastic behavior was identified by its characteristic linear correlation between the duration of, and SD in, the time between oscillation peaks (Fig. 1 *F* and *G*) (43). We also observed repetitive waves of Ca^{2+} signals traveling between individual PSC cells, and the number of cells varied from as few as two cells to, in some instances, over six to seven cells (Fig. 1 *H* and *I* and *SI Appendix*, Fig. S2 *D–F* and Movies S2–S4). On occasion, we also detected Ca^{2+} signals propagating from one cell to two PSC cells simultaneously (*SI Appendix*, Fig. S2*E* and Movie S5). While it is not known whether throughout the entire period of larval life every PSC cell shows Ca^{2+} spikes, it is clear that a significant majority do spike. Specifically, we found that 79% and 83% of PSC cells showed at least one spiking event over the course of 60 and 120 min, respectively (*SI Appendix*, Fig. S2*G*). Moreover, we found that Ca^{2+} signaling was quite uniform in

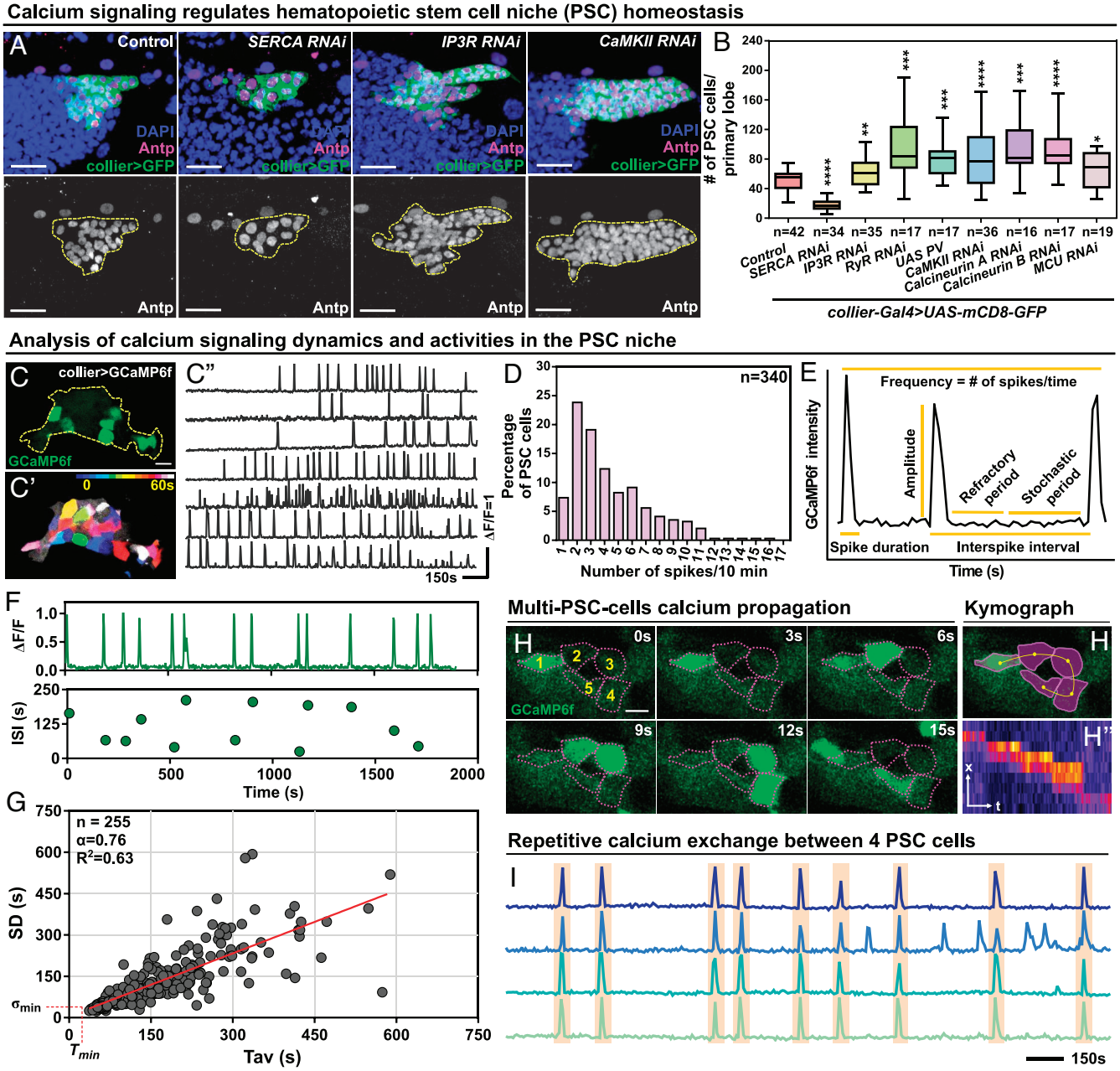

Fig. 1. Spontaneous waves of Ca^{2+} signals regulate PSC homeostasis. (*A* and *B*) Representative images (*A*) and quantification of PSC cell numbers (*B*) in LGs from control and PSC-specific expression of *SERCA-RNAi*, *IP3R-RNAi*, *RyR-RNAi*, *PV*, *CaMKII-RNAi*, *Calcineurin A-RNAi*, *Calcineurin B-RNAi*, and *MCU-RNAi*. PSC labelled with *collier-Gal4*-driven membranous GFP in green and Antp (in red in the top panel and white in the below panel). Nuclei labelled in blue. Sample sizes displayed in (*B*). (*C*–*C″*) Representative image showing a snapshot of GCaMP6f activity in the PSC (*C*). Ca^{2+} signaling activity collected over the 60 s was temporally color-coded in (*C′*). Representative GCaMP6f intensity traces over 45 min from the seven PSC cells in (*C″*). (*D*) Histogram showing the distribution of spiking events per 10 min among n = 340 PSC cells. (*E*) Schematic showing a typical Ca^{2+} spiking activity consists of multiple components including frequency, amplitude, and interspike interval (ISI, consisting of spike, refractory, and stochastic periods) that are used to encode information. (*F*) *Top*: a representative trace showing Ca^{2+} spiking in a PSC cell. *Bottom*: individual lengths of ISI extracted from the above trace. (*G*) A T_{av}-SD plot showing the relationship between the average lengths of ISI (T_{av}) and the SD of data collected from individual PSC cells. T_{min}, refractory period (43). n, number of PSC cells examined. α (slope) and R^2 calculated using linear regression analysis of the T_{av}-SD plot. (*H*–*H″*) Representative images showing multicell Ca^{2+} signaling propagation between five PSC cells visualized using GCaMP6f (Cell #1 to 5; cell borders outlined in magenta) and displayed as a kymograph (*H′* and *H″*). Time in seconds is indicated on the image. (*I*) Representative traces of repetitive Ca^{2+} signaling propagations between four neighboring interconnected PSC cells. Nuclei in (*A*) labeled in blue. GCaMP6f in (*C*) and (*H*) labelled in green. Scale bars in (*A*), (*C*), and (*H*) represent 25, 10, and 5 μm, respectively. Error bars indicate SD of the mean. Genotypes in (*A* and *B*): indicated in the figure. Genotypes in (*C*–*I*): *collier-Gal4>UAS-GCaMP6f*.

the PSC. Specifically, the behavior of Ca^{2+} signaling, in terms of spiking amplitude and frequency, did not vary significantly between PSC cells closer to or further from the cardiac tube or between cells in the anterior or posterior of the LG (*SI Appendix*, Fig. S2 *H*–*K*). Overall, these results showed that robust and stochastic waves of Ca^{2+} are generated and propagated repetitively between PSC cells.

The PSC Niche Is Organized in a Small-World Ca^{2+} Signaling Network. The repeated propagations of Ca^{2+} signals between PSC niche cells suggested that they are linked within a network. To characterize the structure of the Ca^{2+} signaling network in the PSC, we employed a methodology derived from network biology and graph theory (13, 46, 47). Specifically, a cross-correlation analysis and a graph theory approach were applied to identify

cell pairs with highly correlated Ca^{2+} signaling activity (46). A set of data is created that is "scrambled." This is done by shuffling the data of the original Ca^{2+} signals in such a way that the total number of spikes is the same but they are randomized in time (46). Using this scrambled dataset, a cutoff value is derived to filter out at least 99% of random simultaneously occurring Ca^{2+} spikes that take place in adjacent cells (46). Applying such a methodology ensures an objective and nonbiased approach to build a network from recorded Ca^{2+} signals while minimizing the risk of spurious correlations between signaling events due to chance (46). Our analysis of Ca^{2+} activities in the PSC confirmed that the PSC cells were connected in a network (Fig. 2*A*), with individual cells in the network exhibiting distinct levels of correlation with others (Fig. 2*B*). We previously noted for blood progenitors that some of the nodes in a network were multiple cell diameters away from each other (13). As the Ca^{2+} recordings were performed on two focal planes capturing the middle part of the LG, it is possible that there are cells that act as intermediaries to connect these seemingly distant cells together in a 3D network (13). In line with this idea, we observed many examples of Ca^{2+} propagation events involving multiple cells (on average 64 such events were detected per primary lobe imaged, n = 17 videos; Fig. 1 *H* and *I* and *SI Appendix*, Fig. S2 *D–F* and Movies S2–S4). Graph theory–based mathematical descriptions of networks use a set of parameters that include scale-free factor (γ), clustering coefficient (σ), and mean shortest path length (λ) (46–48). The shortest path length is defined as the number of intermediary cells that are on average involved when a signal is transmitted across the network (46, 47). The clustering coefficient is defined as the number of functionally connected neighbors of a cell that are also themselves neighbors, divided by the total number of all possible connections between cell pairs (46, 47). The scale-free factor is the power law exponent that describes the growth and structure of a network (46, 47). When these parameters were calculated for the Ca^{2+} signaling network connecting PSC cells, the values were typical for small-world networks having scale-free topology (Fig. 2*C*) (46). In such a network, some PSC cells have more connections to their neighbors compared to other PSC cells and may be more important for signal propagation (Fig. 2 *C* and *D*) (46–48). One established way of visualizing this feature of a network is to plot the probability

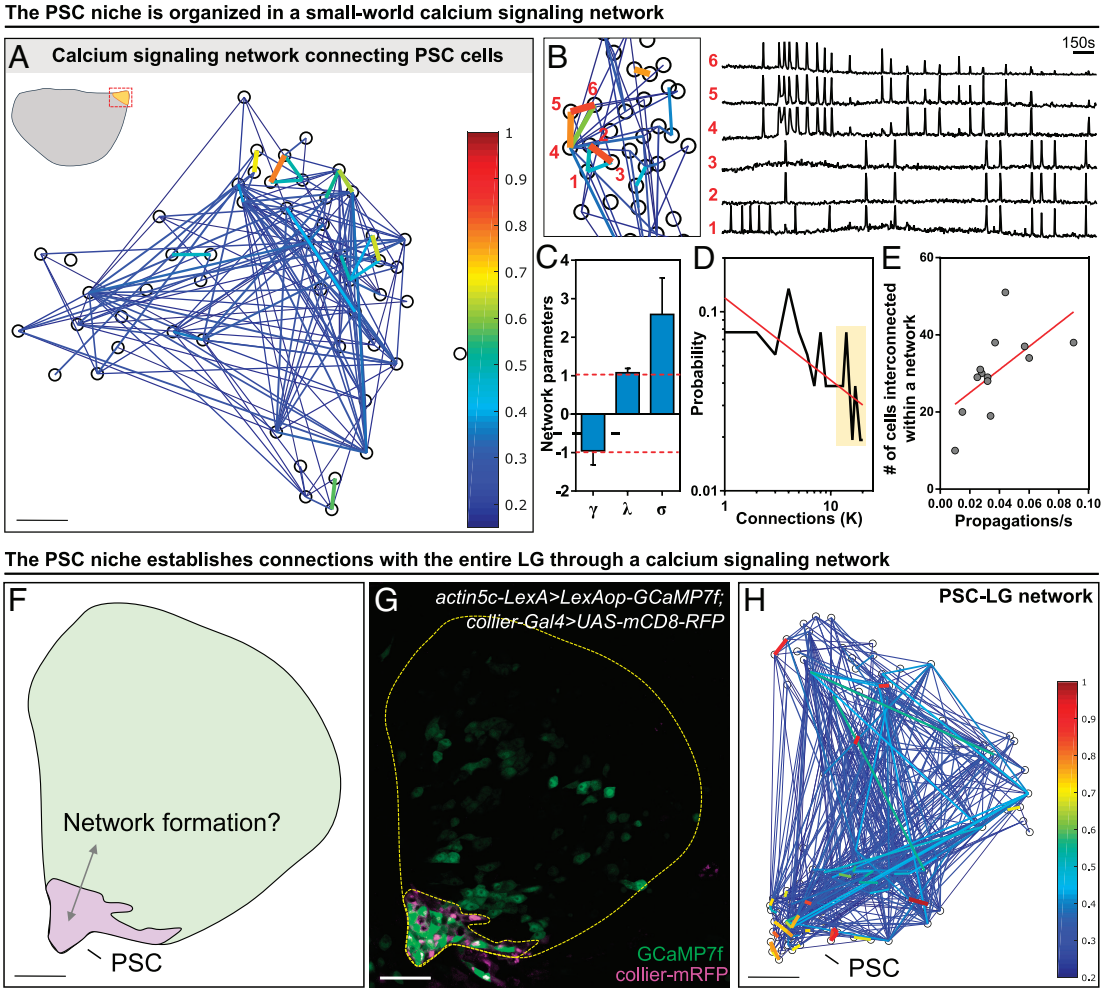

Fig. 2. The PSC niche is organized in a small-world Ca^{2+} signaling network. (*A*) Representative Ca^{2+} signaling network graph constructed in MATLAB using cross-correlation analysis on the Ca^{2+} recordings over 45 min from a PSC niche. Each circle represents a PSC cell that shows a minimum of three spikes (*SI Appendix*). Color-coded legend represents correlation strength. (*B*) *Left panel*: a cluster of PSC cells showing correlation at various levels. *Right panel*: representative Ca^{2+} intensity traces from six PSC cells indicated in the left panel. (*C*) Averaged network parameters including scale-free factor (γ), shortest path length (λ), and clustering coefficient (σ) from a dataset comprising n = 9 PSC videos. (*D*) The scale-free nature of the PSC Ca^{2+} signaling network is confirmed by plotting the number of connections versus probability in a log-log scale (*SI Appendix*). (*E*) A graph showing the positive relationship between the number of Ca^{2+} signaling propagations per second in a PSC niche and the number of cells included in a network. n = 12 PSC videos. (*F* and *G*) Representative schematic (*F*) and confocal (*G*) images showing GCaMP expression in the entire LG using LexA-LexAop system with the PSC labelled by collier-driven membranous mRFP. (*H*) Representative Ca^{2+} signaling network graph showing the PSC establishes robust connections with the entire LG. Genotypes in (*A–E*): *collier-Gal4>UAS-GCaMP6f*. Genotype in (*F–H*): *actin5C-LexA>LexAop-GCaMP7f; collier-Gal4>UAS-mCD8-RFP*. Scale bar in (*A*) and (*F–H*) represents 10 and 40 μm, respectively.

of cells within the network signaling in a concomitant manner (representing cell pairs) versus the number of connections these cells have to other cells (black line in Fig. 2*D*) (46). Our data showed that some cells exhibited a higher number of connections than other cells (Fig. 2*D*). There was also a direct correlation between the number of connections that cells made and the number of propagation events that occurred between these cells (Fig. 2*E*), consistent with Ca^{2+} propagation supporting network formation in the PSC. Taken together, these results suggested that the PSC niche is organized in a small-world Ca^{2+} signaling network.

The Ca^{2+} Signaling Network Extends beyond the PSC to the Medullary Zone. A major function of the PSC in the LG is to regulate blood progenitors in the medullary zone of the LG. We, therefore, asked whether the Ca^{2+} signaling network extended beyond the PSC. To this end, we used the ubiquitous actin5C-LexA driver to express GCaMP throughout the LG while simultaneously labeling the PSC with mCD8-RFP driven by *collier*-Gal4. Network analysis revealed a vast network with robust connections throughout the LG that included cells in both the PSC and the medullary zone (Fig. 2 *F–H*). This raises the possibility that GJ–mediated communication from the PSC to the medullary zone could assist the PSC in regulating blood progenitor cells.

Ca^{2+} Signaling in the PSC Originates from Intracellular ER Ca^{2+} Stores. Ca^{2+} oscillations can occur by the mobilization of intracellular stores initiated by secondary messengers such as IP3 or by the influx of extracellular Ca^{2+} (49–52). By tracking Ca^{2+} oscillations in the PSC of cultured LGs using GCaMP, we observed that knocking down the IP3R, which mobilizes ER stores of Ca^{2+} effectively, abolished all oscillations as very little Ca^{2+} was seen in the cytosol of PSC cells (*SI Appendix*, Fig. S3 *A–C*, and *F* and Movie S6). In comparison, knocking down the Ca^{2+} pump SERCA, which transports Ca^{2+} from the cytosol into the ER, resulted in persistently high levels of Ca^{2+} in the cytosol of PSC cells (*SI Appendix*, Fig. S3 *A*, *B*, *E*, and *L* and Movie S7). Next, the contribution of extracellular Ca^{2+} to oscillations was assessed by treating the cultured LGs with the extracellular Ca^{2+} chelator BAPTA (53). This treatment had no impact on Ca^{2+} signaling in PSC cells (*SI Appendix*, Fig. S3 *A*, *B*, and *D* and Movie S8). These results were consistent with a model whereby Ca^{2+}-signaling in the PSC was predominantly mediated by an intracellular source of Ca^{2+}. We, therefore, analyzed the role of intracellular Ca^{2+} on the signaling network in the PSC. RNAi-mediated knockdown of IP3R strongly reduced the number of PSC cells exhibiting Ca^{2+} oscillations and nearly eliminated signal propagation events between PSC cells (*SI Appendix*, Fig. S3 *F* and *G*). BAPTA treatment, done in parallel, showed no impact on either measurement (*SI Appendix*, Fig. S3 *F* and *G*). A number of network parameters were analyzed following IP3R knockdown including network connectivity, network size, isolation index, and shortest path length. Network connectivity, a measurement of the proportion of cells in a population that is found by cross-correlation network analysis to be part of the signaling network (46), was reduced following IP3R knockdown but not following BAPTA treatment (*SI Appendix*, Fig. S3*H*). Network size, the overall number of PSC cells included in the network (46), was also reduced following IP3R knockdown but not following BAPTA treatment (*SI Appendix*, Fig. S3*I*). In comparison, the isolation index, representing the proportion of cells in the PSC that are completely excluded from the network, was higher following IP3R knockdown but not following BAPTA treatment (*SI Appendix*, Fig. S3*J*). Finally, the shortest path length, which measures how efficiently information is transferred in a network (46), was also substantially decreased following IP3R knockdown (*SI Appendix*, Fig. S3*K*). Based on these data, we concluded that an intracellular rather than an extracellular source underlies Ca^{2+} oscillations in the PSC cells and facilitates the formation of a signaling network.

GJ-Mediated Communication Establishes the Ca^{2+} Signaling Network in the PSC. The propagation of intracellular Ca^{2+} between cells can be mediated through GJs (13, 28, 54–56). To determine whether GJs were involved in the formation of the Ca^{2+} signaling network in the PSC, the gap-junction blocker carbenoxolone (CBX) was added to ex vivo cultured LGs. Cross-correlation and network analyses showed that treatment with CBX greatly reduced Ca^{2+} oscillations and disrupted the Ca^{2+} signaling network in the PSC (Fig. 3 *A–C* and Movies S9 and S10). Washing out the CBX from the culture media resulted in a resumption of Ca^{2+} oscillations and partial recovery of the Ca^{2+} signaling network (Fig. 3 *A–C* and Movie S11). Quantification of the number of PSC cells showing Ca^{2+} oscillations as well as the number of propagation events showed that both parameters were reduced by CBX treatment in a dose-dependent manner (Fig. 3 *B* and *C*). For both parameters, the effect was reversed by washing out the CBX drug out of the culture media (Fig. 3 *B* and *C*). Analysis of other quantitative measurements of the network illustrated the disruptive effect of CBX including decreased network connectivity (Fig. 3*D*), a smaller network size (Fig. 3*E*), a higher isolation index (Fig. 3*F*), a lower shortest path length (Fig. 3*G*), and a reduced clustering coefficient (Fig. 3*H*). These changes could be partially reversed within minutes of washing to remove the CBX drug from the culture media (Fig. 3 *B–H*). These data pointed to a crucial role for GJs in Ca^{2+} signaling and network formation in the PSC.

GJs Maintain Niche Homeostasis and the Ca^{2+} Signaling Network. Since GJs control Ca^{2+} signaling in the PSC, which in turn controls niche homeostasis, we investigated the consequences of PSC-specific knockdown of the expression of all eight innexins encoded in the fly genome (31, 32). RNAi-mediated knockdown of the three innexins, *inx1* (also known by its gene name *ogre*), *inx3*, and *inx8* (also known by its gene name *shakB*), resulted in a significant increase in the PSC size while knockdown of *inx2*, *inx4/zpg*, *inx5*, *inx6*, and *inx7* showed no impact on the PSC size (Fig. 4 *A–C*). To confirm the presence of GJs in the PSC, we performed electron microscopy and were able to observe the presence of extensive GJ plaques connecting individual PSC cells (an example of a GJ plaque is shown in Fig. 4*D*) (57). To determine which of the three innexins (Inx1/Ogre, Inx3, or Inx8/ShakB) controlled Ca^{2+} signaling in the PSC, we combined innexin knockdown with live imaging to visualize Ca^{2+} using GCaMP in ex vivo LGs. Specifically, RNAi-mediated knockdown of *ogre*/*inx1* in the PSC showed severe disruption of the Ca^{2+} signaling network (Fig. 4 *F* and *I* and Movies S12–S14). In comparison, PSC-specific RNAi-based knockdown of *inx3*, *shakB*/*inx8*, or a double knockdown of both *inx3* and *shakB*/*inx8* caused a much lesser disruption to the Ca^{2+} signaling network in the PSC (Fig. 4 *F* and *I*). Subsequent analysis of other quantitative measurements of the network was carried out to determine the role of Ogre/Inx1, Inx3, or ShakB/Inx8 in maintaining the Ca^{2+} signaling network in the PSC (Fig. 4 *G–L*). Specifically, the depletion of Ogre/Inx1 resulted in a smaller number of oscillating cells (Fig. 4*G*), a decreased number of Ca^{2+} propagation events (Fig. 4*H*), a reduced network connectivity (Fig. 4*I*), a smaller network size (Fig. 4*J*), a higher isolation index (Fig. 4*K*), and a lower shortest path length (Fig. 4*L*). However, PSC-specific knockdown of *inx3*, *shakB*/*inx8*, or a double

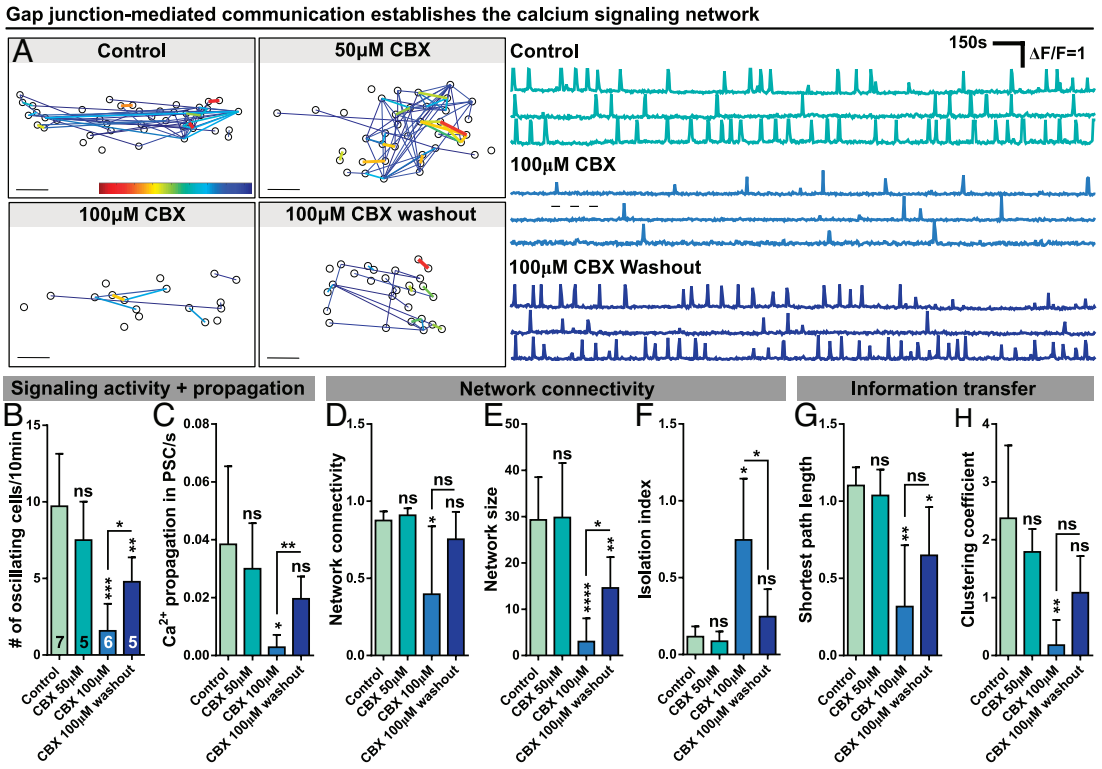

Fig. 3. GJ-mediated communication establishes the Ca^{2+} signaling network. (*A*) Representative network images (*Left*) and Ca^{2+} intensity traces over 45 min (*Right*) of PSCs from control (without CBX), 50 μM CBX treatment, 100 μM CBX treatment, and CBX washout experiments. (*B–H*) Quantification of the number of oscillating PSC cells (*B*), number of Ca^{2+} signaling propagations per second (*C*), network connectivity (*D*), network size (*E*), isolation index (*F*), shortest path length (*G*), and clustering coefficient (*H*) of PSCs from control (without CBX), CBX treatment at different concentrations (50 and 100 μM), and CBX washout groups. Genotype of LGs: *collier-Gal4>UAS-GCaMP6f*. Sample sizes (n = number of PSC videos) displayed on the graph. Scale bars in (*A*) represent 10 μm. Error bars indicate SD of the mean.

knockdown of both *inx3* and *shakB*|*inx8* either did not impact or caused a much milder effect than *ogre*|*inx1* knockdown on the network structure and parameters (Fig. 4 *G–L*). Moreover, using immunohistochemistry to visualize Ogre/Inx1-based GJs, we detected many Ogre/Inx1 plaques, appearing as puncta, in between PSC cells, though its expression was not limited to the PSC and could be detected throughout the LG (Fig. 4 *E–E″* and *SI Appendix*, Fig. S4 *A* and *B*). These data showed that Ogre/Inx1-based GJs maintained the Ca^{2+} signaling network in the PSC and consequently niche homeostasis. In line with the hypothesis that Ogre/Inx1-mediated Ca^{2+} signals played a unique role in niche homeostasis, knockdown of *ogre*|*inx1* in the PSC led to an increased number of plasmatocytes but not crystal cells and a decreased blood progenitor maintenance (*SI Appendix*, Fig. S1 *A*, *D–G*). However, knockdown of *inx2* (as an internal control: knockdown of which affected neither PSC size nor Ca^{2+} signaling), *inx3, shakB*|*inx8* (knockdown of which affected only PSC size but not Ca^{2+} signaling), or a double knockdown of both *inx3* and *shakB*|*inx8* did not affect plasmatocyte differentiation (*SI Appendix*, Fig. S1*E*). One important caveat was that the *colliar-Gal4* is also expressed in the central nervous system (CNS) (58) and we could not discount the possibility that Ogre/Inx1 functions in the CNS which could, through some unspecified mechanisms, impact LG homeostasis. To address this caveat, we carried out experiments where we combined the *colliar-Gal4* driver with the *nSyb-Gal80* transgene (59) that is designed to inhibit Gal4 activity in the nervous system. We confirmed that introducing the *nSyb-Gal80* transgene worked to suppress Gal4-dependent GFP expression in the CNS (*SI Appendix*, Fig. S5 *A–C*). Importantly, introducing the *nSyb-Gal80* transgene did not modify the PSC overgrowth (*SI Appendix*, Fig. S5 *D–G*) and plasmatocyte differentiation (*SI Appendix*, Fig. S1*E*) phenotypes induced by *ogre*|*inx1* knockdown. These results confirmed that Ogre/Inx1-based GJs maintain niche size and LG homeostasis.

Ogre-Based GJs Control the Spiking Frequency and Amplitude of Ca^{2+} to Maintain Niche Homeostasis. Ca^{2+} signaling provides a mechanism to encode and transmit information and GJs allow this Ca^{2+}-encoded information to be propagated between cells (55, 60–62). Ca^{2+}-encoded information can take the form of changes in the amplitude and/or frequency of Ca^{2+} oscillations (60–62). In the PSC, knockdown of *ogre*|*inx1*, but not *inx3* or *shakB*|*inx8*, altered the amplitude and frequency of Ca^{2+} signals (Fig. 5 *A–C*). In particular, knockdown of *ogre*|*inx1* in the PSC resulted in a reduced Ca^{2+} oscillation frequency, due to a higher percentage of PSC cells exhibiting nearly no oscillations, and an increased average Ca^{2+} spike amplitude (Fig. 5 *A–C*). The effect of RNAi-mediated knockdown of *ogre*|*inx1* on the frequency and amplitude of Ca^{2+} oscillations can be reproduced by treatment with the GJ blocker CBX, and this effect was reversible by washing out the CBX drug (Fig. 5 *D* and *E*). This suggested that most if not all of the Ca^{2+}-encoded information in the PSC was mediated and transferred by Ogre/Inx1-based GJs. Consistent with this observation, PSC-specific knockdown of IP3R induced similar effects on Ca^{2+} oscillation frequency and spike amplitude to those observed in either knockdown of *ogre*|*inx1* in the PSC or CBX treatment (Fig. 5*F*). The changes in Ca^{2+}-encoded information we observed would be predicted to impact downstream Ca^{2+} signaling. To test this hypothesis, we measured the fluorescent intensity of CaLexA, which represents the levels of persistent Ca^{2+} signaling activity, in the PSC (Fig. 5 *G–I*). Knockdown of *ogre*|*inx1* in the PSC, but not knockdown of *inx3* or *shakB*|*inx8*,

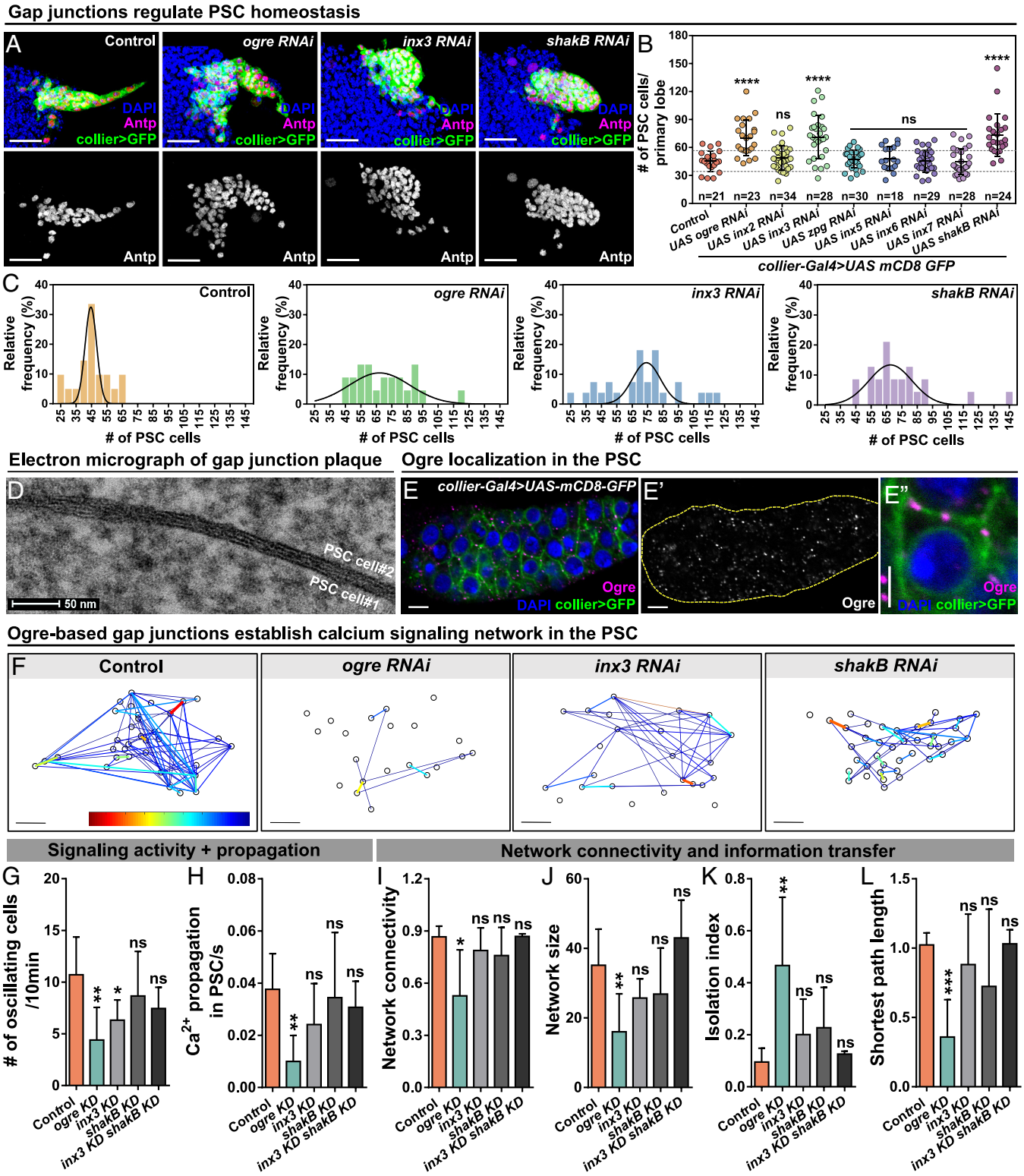

Fig. 4. GJs maintain PSC homeostasis and Ca^{2+} signaling network. (*A* and *B*) Representative images (*A*) and quantification of the number of PSC cells (*B*) in LGs of control and following PSC-specific RNAi-mediated knockdown of eight *Drosophila* innexins. PSC labelled with collier-Gal4 driven membranous GFP (in green) and Antp (in red in the top panel and white in the below panel). Dash lines in (*B*) represent the SD range of control. (*C*) Histogram analysis performed on data from (*B*) including control, PSC-specific *ogre* knockdown, *inx3* knockdown, and *shakB* knockdown groups. Sample sizes (n = number of PSCs analyzed) displayed in (*B*). (*D*) Electron micrograph of a GJ plaque in the PSC. (*E*) Representative image showing Ogre localization in the PSC. PSC labelled with collier-Gal4 driven membranous GFP. Ogre labelled in magenta. Nuclei labelled in blue. (*F*) Representative network images of PSCs from LGs of control, PSC-specific *ogre* knockdown, PSC-specific *inx3* knockdown, and PSC-specific *shakB* knockdown. The color legend indicates correlation strength. (*G–L*) Quantification of the number of oscillating PSC cells (*G*), number of Ca^{2+} signaling propagations per second (*H*), network connectivity (*I*), network size (*J*), isolation index (*K*), and shortest path length (*L*) from LGs of control (n = 6 videos), PSC-specific *ogre* knockdown (n = 7 videos), PSC-specific *inx3* knockdown (n = 7 videos), PSC-specific *shakB* knockdown (n = 7 videos), and PSC-specific knockdown of both *inx3* and *shakB* (n = 4 videos). Genotypes indicated on the graphs. Scale bars in (*A*), (*D*), (*E*), (*E″*), and (*F*) represent 25 μm, 50 nm, 5 μm, and 10 μm, respectively.

caused a reduction in the sustained downstream response to Ca^{2+} signals in the PSC as judged by CaLexA expression (Fig. 5 *G–I*). Importantly, the increased size of the PSC observed following PSC-specific depletion of Ogre/Inx1 was largely rescued by elevating the cytosolic levels of Ca^{2+} through knockdown of the SERCA pump (Fig. 5 *J–L*). Taken together, these data suggested that Ogre/Inx1-based GJs regulate the frequency and amplitude of Ca^{2+} oscillations in the PSC which controls the level of Ca^{2+} signaling in the niche and consequently its homeostasis.

GJ-Mediated Ca^{2+} Signaling Modulates the Hedgehog Pathway to Maintain Blood Cell Homeostasis. Since our data showed that the downstream Ca^{2+} effector CaMKII regulated PSC niche homeostasis (Fig. 1 *A* and *B*), we asked whether CaMKII activity was controlled by GJs. To this end, an antibody that detects active, phosphorylated, CaMKII was used to stain control LGs and LGs in which Ogre/Inx1 was depleted from the PSC using RNAi. In control, phosphorylated CaMKII appeared as puncta dispersed throughout the PSC. This pattern was substantially reduced, by over 50%, in PSC cells where Ogre/Inx1 was depleted (Fig. 6 *A–C*, *C′*). The data (Figs. 1 *A* and *B* and 6 *A–C*) suggested that Ogre/Inx1 GJs control CaMKII activity to regulate PSC size.

As the major role of the PSC is to maintain blood cell homeostasis in the LG, we next asked whether other niche-derived signaling pathways that have been shown to control the function of the PSC and the behavior of blood progenitors were regulated by Ogre/Inx1-based GJs. The Dpp/BMP and Wg pathways act in the PSC to determine the size of the niche and also non-cell-autonomously regulate blood progenitors (18) while the Hh pathway is a key signal produced by the PSC cells to regulate blood progenitor maintenance and differentiation (15). An antibody that detects phospho-MAD (pMad) was used as a marker to analyze Dpp/BMP activity in the niche (Fig. 6*D*) while a specific antibody was used to detect the Wg ligand (Fig. 6*F*). In addition, to detect Hh expression, we utilized a transgene that expresses GFP under the control of an enhancer sequence, called hhF4f, that is known to specifically mediate Hh expression in the PSC (Fig. 6*H*) (63). This analysis demonstrated that following loss of Ogre/Inx1-based GJs in the PSC, Wg and Dpp/BMP pathway activities were similar to those in controls (Fig. 6 *D*, *E*, and *J* for Dpp/BMP; Fig. 6 *F*, *G*, and *K* for Wg) while hhF4f driven GFP intensity was strongly reduced following depletion of Ogre/Inx1 from the PSC (Fig. 6 *H*, *I*, and *L*). Next, we directly visualized Hh ligands in the PSC and found that, compared to controls, there was a marked reduction in the level of Hh ligands following knockdown of *ogre/inx1* but not following double knockdown of *inx3* and *shakB/inx8* (*SI Appendix*, Fig. S6 *A*, *B*, and *D*). These results suggested that Hh signaling is transcriptionally regulated downstream of Ogre/Inx1-based GJs in the PSC but did not directly link changes in Hh signaling to Ca^{2+} signaling. Moreover, we may expect that changes in the Hh pathway in the PSC would impact progenitors. To study these directly, we knocked down the expression of either *ogre/inx1* or CaMKII in the PSC using RNAi and asked whether Hh pathway activity in the LG, visualized using an antibody that detects the activated form of the downstream Hh effector Cubitus interruptus (Ci^{act}), was altered (Fig. 6 *M–O*). Subsequent to knockdown of either *ogre/inx1* or CaMKII in the PSC, we observed a substantial reduction in Ci expression in the regions where blood progenitors reside compared to that in controls (yellow arrows, Fig. 6 *M–O*). Consistent with the decreased Hh signaling activity, depletion of Ogre/Inx1 or Ca^{2+} all resulted in significant plasmatocyte differentiation (*SI Appendix*, Fig. S1 *A–E*). Finally, we found that ectopically expressing Hh in the PSC or, alternatively, elevating Ca^{2+} levels in the Ogre/Inx1-depleted PSC cells using RNAi-mediated knockdown of *SERCA* rescued the reduction in Hh levels (*SI Appendix*, Fig. S6 *A*, *C*, and *E*) as well the plasmatocyte differentiation associated with *ogre/Inx1* depletion (*SI Appendix*, Fig. S1*E*). Taken together, these results suggested that Ogre/Inx1-based GJs facilitate Ca^{2+} signaling, through CaMKII, to control PSC homeostasis and modulate the amount of Hh produced by the niche to regulate blood progenitor maintenance (summarized as a working model in *SI Appendix*, Fig. S7).

Discussion

Here, we have shown that modulating Ca^{2+} levels and/or Ca^{2+} signaling in the PSC affects niche homeostasis and blood cell differentiation. Specifically, we found that spontaneous and stochastic waves of Ca^{2+} are propagated between PSC cells. The propagation of Ca^{2+} between cells established a Ca^{2+} signaling network within the PSC niche. We went on to show that the source of Ca^{2+} oscillations between PSC cells was intracellular rather than extracellular and required GJs. In particular, Ogre/Inx1-based GJs were identified as essential for the formation of the Ca^{2+} signaling network within the PSC. Phenotypic analysis of the role of Ogre/Inx1-based GJs in the PSC niche revealed they were required to regulate the frequency and amplitude of Ca^{2+} oscillations in the PSC and that this controlled the level of Ca^{2+} signaling in the niche and consequently its homeostasis. Finally, analysis of various cell signaling pathways in the PSC showed that the CaMKII and Hh pathways act downstream of GJ-mediated Ca^{2+} signaling in the niche to regulate PSC homeostasis and blood progenitor maintenance, respectively.

We have previously described a GJ and Ca^{2+} signaling-based mechanism that coordinates cell fate decisions in the blood progenitors (13). While there are certain similarities between the blood progenitors and the PSC in using this regulatory strategy, there are notable mechanistic differences. First, different innexins are used in GJs in the PSC and blood progenitors. While blood progenitors utilize Zpg/Inx4 to communicate with each other (13), PSC cells use three different innexins, Ogre/Inx1, Inx3, and ShakB/Inx8 of which Ogre/Inx1 is most strongly associated with the formation of the Ca^{2+} signaling network. Second, the Ca^{2+} encoding operates differently in the PSC and blood progenitors. Disrupting GJs in the blood progenitors increased the frequency and decreased the amplitude of Ca^{2+} oscillations (13) while disrupting GJs in the PSC had the opposite effect, decreasing the frequency and increasing the amplitude. Third, the source of Ca^{2+} used in the blood progenitors and the PSC is different. Blood progenitors use both intracellular and extracellular Ca^{2+} (13), while the PSC mainly utilizes intracellular Ca^{2+}. In particular, our data suggest that Ogre/Inx1-based GJs control Ca^{2+} signaling in the PSC through IP3 as the IP3R is required to maintain the Ca^{2+} signaling network. Notably, knockdown of IP3R leads to a similar impact on the Ca^{2+} signaling network in the PSC as knockdown of *ogre/inx1*, but not *inx3* or *shakB/inx8*. Since IP3 is a well-known cargo that moves through GJs (49), consistent with our data, we propose that it is a major cargo transported by Ogre/Inx1 between PSC cells.

The observation that Inx3 and ShakB/Inx8 were both required for PSC maintenance but were not essential for the formation of the Ca^{2+} signaling network suggested that they either function redundantly in transporting Ca^{2+} or that they form GJs that are mainly responsible for transporting cargoes other than Ca^{2+}. In comparison, Ogre/Inx1 was shown to have a unique and central role in the PSC in forming the Ca^{2+} signaling network and in maintaining niche homeostasis. When considered with our previous data (13), these results suggest that there are multiple types of GJs, heterotypic or homotypic, operating in the LG and that they mediate communication between different cell types in the

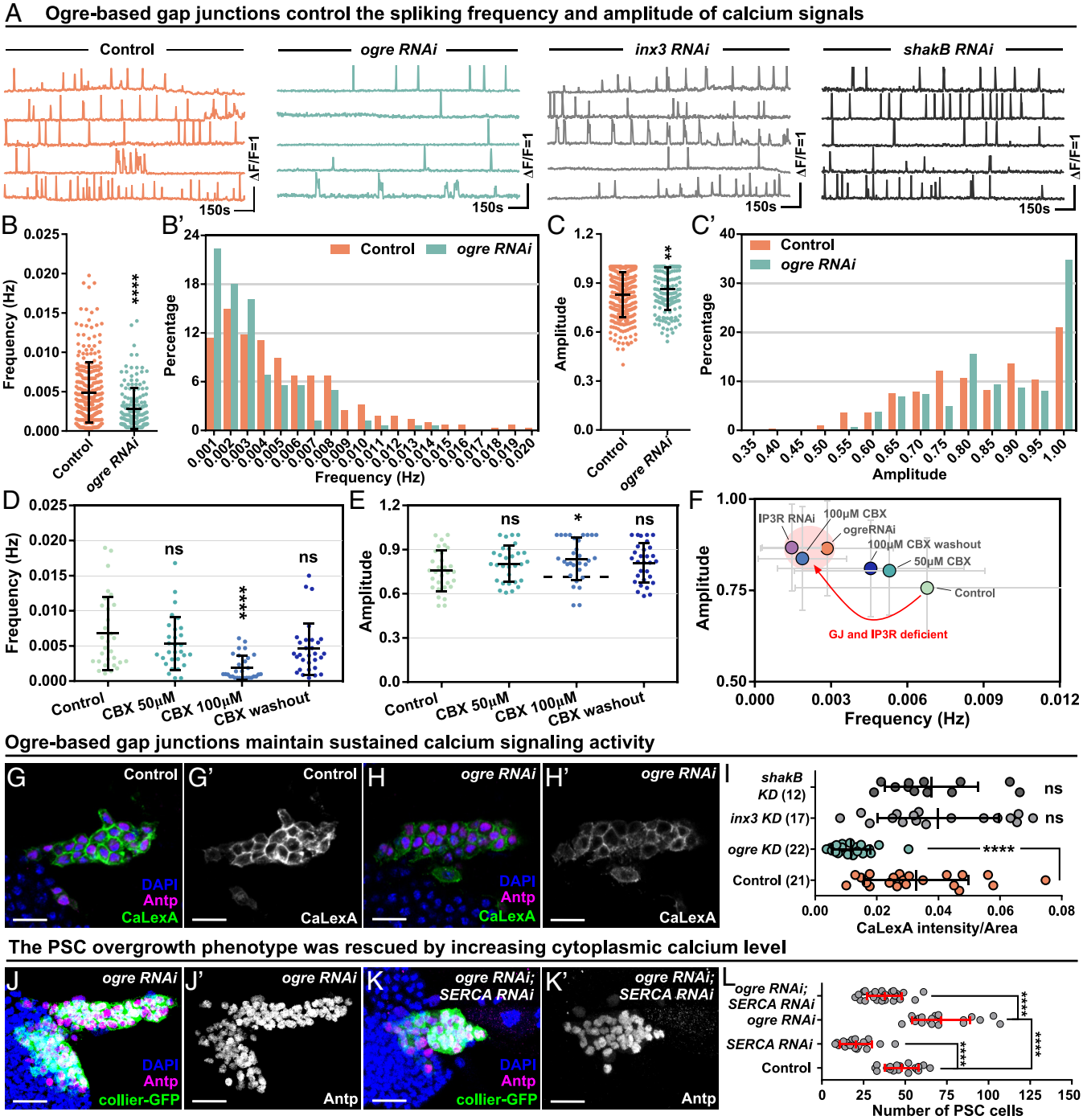

Fig. 5. Ogre-based GJs control the spiking frequency and amplitude of Ca^{2+} to maintain niche homeostasis. (*A*) Representative Ca^{2+} intensity traces of PSC cells from LGs of control (genotype: *collier-Gal4>UAS-GCaMP6f*), PSC-specific *ogre* knockdown (genotype: *collier-Gal4>UAS-GCaMP6f>UAS-ogre-RNAi*), PSC-specific *inx3* knockdown (genotype: *collier-Gal4>UAS-GCaMP6f>UAS-inx3-RNAi*), and PSC-specific *shakB* knockdown (genotype: *collier-Gal4>UAS-GCaMP6f>UAS-shakB-RNAi*). (*B* and *B′*) Quantification (*B*) and histogram analysis (*B′*) of Ca^{2+} spiking frequency (unit: Hz) in PSC cells from LGs of control (n = 280 PSC cells) and PSC-specific *ogre* knockdown (n = 161 PSC cells). (*C* and *C′*) Quantification (*C*) and histogram analysis (*C′*) of Ca^{2+} spiking amplitude (unit: a.u) in PSC cells from LGs of control (n = 280 PSC cells) and PSC-specific *ogre* knockdown (n = 161 PSC cells). (*D* and *E*) Quantification of Ca^{2+} spiking frequency (*D*) and amplitude (*E*) in PSC cells from LGs of control (without CBX, n = 30 PSC cells), CBX treatment at different concentrations (50 and 100 μM, n = 30 PSC cells in both groups), and CBX washout groups (n = 30 PSC cells). (*F*) Visualizing a switch in Ca^{2+} signaling patterns in PSC cells upon different treatments (including control, PSC-specific *ogre* and *IP3R* knockdown, 50 and 100 μM CBX treatment, and CBX washout) by plotting spiking frequency against spiking amplitude (40). (*G–I*) Representative images and quantification showing sustained Ca^{2+} signaling in PSC cells from LGs of control (*G* and *G′*, *I*, n = 21 primary lobes, genotype: *collier-Gal4>UAS-CaLexA*), PSC-specific *ogre* knockdown (*H* and *H′*, *I*, n = 22 primary lobes, genotype: *collier-Gal4>UAS-CaLexA>UAS-ogre-RNAi*), PSC-specific *inx3* knockdown (*H* and *H′*, *I*, n = 17 primary lobes, genotype: *collier-Gal4>UAS-CaLexA>UAS-inx3-RNAi*), and PSC-specific *shakB* knockdown (*H* and *H′*, *I*, n = 12 primary lobes, genotype: *collier-Gal4>UAS-CaLexA>UAS-shakB-RNAi*) visualized by the CaLexA system (green in *G* and *H*; white in *G′*, *H′*). PSC labelled with Antp (magenta). (*J–L*) Representative images and quantification (*L*) showing the number of cells contained in a PSC from LGs of control (*L*, n = 18 primary lobes, genotype: *collier-Gal4>UAS-mCD8-GFP*), PSC-specific ogre knockdown (*J* and *J′*, *L*, n = 19 primary lobes, genotype: *collier-Gal4>UAS-mCD8-GFP>UAS-ogre-RNAi*), PSC-specific *SERCA* knockdown (*L*, n = 17 primary lobes, genotype: *collier-Gal4>UAS-mCD8-GFP>UAS-SERCA-RNAi*), and PSC-specific *ogre* and *SERCA* knockdown (*K* and *K′*, *L*, n = 27 primary lobes, genotype: *collier-Gal4>UAS-mCD8-GFP>UAS-ogre-RNAi>UAS-SERCA-RNAi*). PSC labelled with collier-Gal4 driven membranous GFP (green) and Antp (magenta in *J* and *K*; white in *J′* and *K′*). Scale bars in (*G* and *H*) and (*J* and *K*) represent 20 μm.

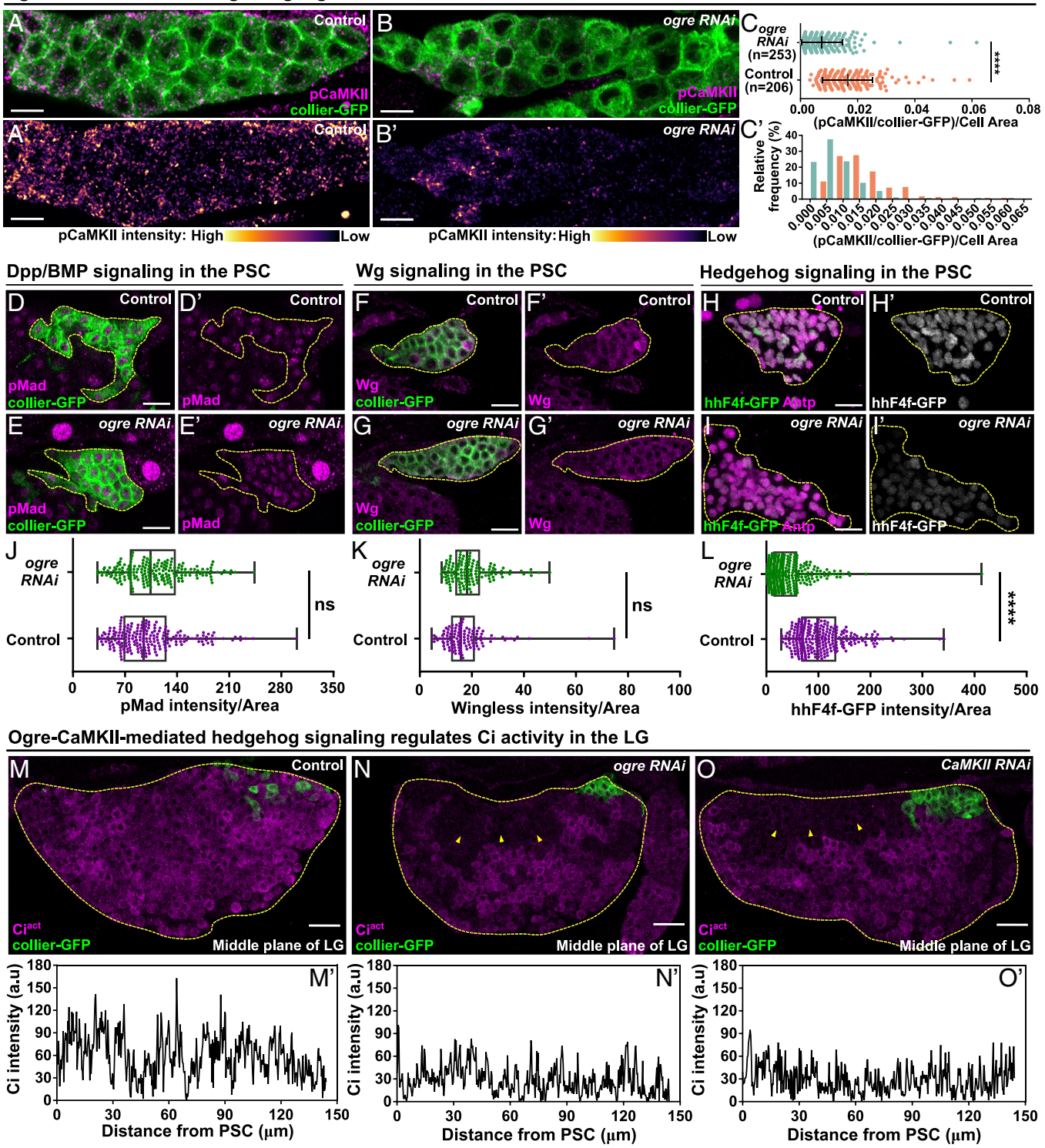

Fig. 6. GJ-mediated Ca^{2+} signaling modulates CaMKII activation and the Hedgehog signaling pathway to maintain PSC and blood cell homeostasis. (*A–C*) Representative images (*A* and *B*) and quantification (*C* and *C′*) of the activity of CaMKII in the PSCs from LGs of control (*A*, n = 206 PSC cells, genotype: *collier-Gal4>UAS-CD8-GFP*) and PSC-specific *ogre* knockdown (*B*, n = 253 PSC cells, genotype: *collier-Gal4>UAS-CD8-GFP>UAS-ogre-RNAi*). Activated CaMKII labelled in magenta in (*A* and *B*). PSC labelled with collier-Gal4 driven membranous GFP. Color legend indicates the level of pCaMKII staining in (*A′*) and (*B′*). (*D-I*) Representative images showing Dpp/BMP signaling (*D* and *E*; pMad in magenta), Wg signaling (*F* and *G*; Wg in magenta), and hedgehog signaling (*H* and *I*; hhF4f-GFP in green in *H* and *I*, and in white in *H′* and *I′*) activity in the PSCs from LGs of control and PSC-specific ogre knockdown. (*J*) Quantification of Dpp/BMP signaling activity in the PSCs from LGs of control (n=209 PSC cells, genotype: *collier-Gal4>UAS-CD8-GFP*) and PSC-specific *ogre* knockdown (n=197 PSC cells, genotype: *collier-Gal4>UAS-CD8-GFP>UAS-ogre-RNAi*). (*K*) Quantification of Wg signaling activity in the PSCs from LGs of control (n=120 PSC cells, genotype: *collier-Gal4>UAS-CD8-GFP*) and PSC-specific *ogre* knockdown (n=140 PSC cells, genotype: *collier-Gal4>UAS-CD8-GFP>UAS-ogre-RNAi*). (*L*) Quantification of hedgehog signaling activity in the PSCs from LGs of control (n=253 PSC cells, genotype: *hhF4f-GFP; collier-Gal4*) and PSC-specific *ogre* knockdown (n=285 PSC cells, genotype: *hhF4f-GFP; collier-Gal4>UAS-ogre-RNAi*). (*M–O*) Representative images and quantification of Ci level and intensity profiles in the LGs from control (*M* and *M′*, genotype: *collier-Gal4>UAS-CD8-GFP*, n = 10 primary lobes), PSC-specific *ogre* knockdown (*N* and *N′*, genotype: *collier-Gal4>UAS-CD8-GFP>UAS-ogre-RNAi*, n = 8 primary lobes), and PSC-specific *CaMKII* knockdown (*O* and *O′*, genotype: *collier-Gal4>UAS-CD8-GFP>UAS-CaMKII-RNAi*, n = 12 primary lobes). Ci labelled in magenta (the activated form of Ci labelled as Ci^{act}). Ci intensity profile is measured by drawing a ROI along the dorsal vessel that is 3-cells wide starting from the PSC until the anterior end of the LG (*SI Appendix*). PSC is labelled with collier-Gal4 driven membranous GFP (green in *A–B*, *D–G*, and *M–O*) and Antp (magenta in *H–I*). Scale bars in (*A–B*), (*D–G*), and (*M–O*) represent 5, 10, and 20 μm, respectively.

LG, often in a redundant fashion. What is particularly notable about the loss of Ogre/Inx1 in the PSC is the way it impacts Ca^{2+} encoded signals, changing both their frequency and amplitude. It has been shown that the function of the Ca^{2+} signaling effector CaMKII is modulated by the frequency and amplitude of Ca^{2+} signals (64). Together with our data, we propose a model that niche homeostasis requires the maintenance of a consistent level of CaMKII activation mediated by Ca^{2+} signaling across the PSC, a requirement that is achieved by equilibrating the levels of Ca^{2+} between PSC cells through GJs. Such a model would be in line with our observation that PSC-derived Hh signals are controlled by modulation of CaMKII function in the PSC. Hh signaling has a well-established and conserved role in the regulation of adult tissue homeostasis and repair (65). In particular, Hh signaling has been shown in diverse systems, including bone, muscle, gut, and hematopoiesis in vertebrates, to be a key regulator of stem cell and progenitor cell behaviors (65). By placing the Hh pathway downstream of GJ-mediated Ca^{2+} signaling in the PSC, we uncover a potential mechanism that links GJs and tissue homeostasis during hematopoiesis.

Our study also points to an intriguing correlation between niche size and blood progenitor homeostasis. Specifically, we found that loss of GJs or Ca^{2+} signaling in the PSC leads to niche overgrowth and increased blood cell differentiation. Since the niche typically secretes signals that maintain blood progenitor homeostasis, it does not necessarily follow that increased blood cell differentiation would result from an increase in niche size. Previous studies on genetic backgrounds that expand the size of the PSC niche provide some insight into possible explanations. For example, it has been shown that loss of Dpp/BMP signaling in the niche gives rise to an enlarged niche that suppresses blood cell differentiation in the LG (18). This phenotype was explained by the ability of Dpp/BMP to suppress the activity of Wg signaling in the niche, which increases the number of PSC cells that can secrete more maintenance signals that inhibit blood cell differentiation (18). We observed the exact opposite result to Dpp/BMP depletion (18) when Ogre/Inx1 is knocked down in the niche: An increased niche size and subsequently increased blood cell differentiation. However, this difference can be explained by the observation that neither Dpp/BMP nor Wg signaling appear altered following the knockdown of Ogre/Inx1 in the PSC. Taken together, these observations suggest that there is no strict correlation between PSC size and the level of blood cell differentiation. Rather, what matters is the impact each genetic background has on the signals produced by the PSC niche. This is in line with some previous findings showing that RNAi-mediated knockdown of *collier* in the PSC had no impact on LG homeostasis (18) as well as studies showing that even ablation of the entire PSC had little impact on blood cell homeostasis (16, 66). In addition, since cells in the PSC niche secrete signals that both promote and suppress blood progenitor differentiation (9), this hints at the ability of niche cells to fine-tune the amount of signal they individually produce to compensate for changes in niche size. Finally, we suggest that there are multiple mechanisms that control PSC niche size, a Dpp/BMP-Wg-dMyc pathway (18), and a GJs-Ca^{2+}-network-CaMKII pathway.

The signaling environment in the LG is extremely complex (10). For example, signals that originate from the PSC, blood progenitors, and differentiated blood cells regulate each other synergistically (22). Because of this, we cannot currently resolve whether the GJ-mediated Ca^{2+} signaling network in the PSC functions upstream or downstream of signals coming from other cell populations in the LG. This is a particularly difficult problem to solve because of the dynamic nature of the LG, but it is an open question worth future investigations. In addition, tissues outside of the LG such as the cardiac tube might impact Ca^{2+} signaling in the LG. For example, the cardiac tube has been shown to be a source of the secreted ligand Branchless which may activate its receptor Breathless in the PSC to induce intracellular Ca^{2+} release (67). Finally, we focused our work primarily on the differentiation of plasmatocytes. Our future work will extend this analysis to lamellocytes and crystal cells. Nonetheless, the substantial impacts that the change in niche homeostasis can have on plasmatocyte differentiation are consistent with this being a key mechanism for regulating hematopoiesis. For example, modulating niche homeostasis offers the ability for systemic signals to have a large and sustained influence on hematopoiesis. The existence of a signaling network between PSC cells ensures a rapid and well-coordinated response to systemic cues.

Materials and Methods

***Drosophila* Genetics and Stocks.** All *Drosophila* stocks and crosses were maintained on standard cornmeal medium in vials or bottles at 25 °C. *Drosophila* stocks were listed in *SI Appendix*, Table S1 and *SI Appendix*.

Antibodies and Immunohistochemistry. Antibodies and detailed immunostaining protocols were provided in *SI Appendix*.

Ex Vivo LG Culture and Confocal Microscope. LGs were cultured ex vivo and imaged using the published procedure (13) detailed in *SI Appendix*.

Ca^{2+} Imaging and Analysis. Ca^{2+} imaging and analyses were performed following the published procedure (13) detailed in *SI Appendix*.

Pharmacological Drug Treatment. CBX (Sigma, CG4790) and BAPTA (ThermoFisher Scientific, B1204) were applied following the procedure detailed in *SI Appendix*.

Network Analysis. Network analysis was performed following the published procedure (13, 46) detailed in *SI Appendix*.

Data Collection and Quantification. Quantification of immunofluorescent intensities of CaLexA, pCaMKII, pMad, Wg, and hhF4f, as well as the Ci intensity profile, number of $Antp^{+}$ PSC cells, plasmatocyte and crystal cells differentiation, and progenitor maintenance are detailed in *SI Appendix*. The electron microscope was performed by W.V. following the standard published detailed protocol (26).

Statistical Analysis. *P* values were determined using a two-tailed unpaired Student *t* test, and Welch's correction was applied. **** indicates $P < 0.0001$, *** indicates $P < 0.001$, ** indicates $P < 0.01$, * indicates $P < 0.05$, ns (non-significant) indicates $P > 0.05$. Error bars indicate SD of the mean. The sample size of each analysis is indicated in figure legends.

Data, Materials, and Software Availability. Further information and requests for resources and reagents should be directed to and will be fulfilled by the lead contact, Guy Tanentzapf (tanentz@mail.ubc.ca). All materials used in this study are documented in *SI Appendix*, Table S1. All the MATLAB scripts used for network analysis and calculating the number of plasmatocytes as well as the total number of cells in a LG are publically available from the published articles (13, 26, 46). All other data are included in the manuscript and/or supporting information.

ACKNOWLEDGMENTS. We acknowledge the Bloomington *Drosophila* Stock Center, the Vienna *Drosophila* Resource Center, and the Developmental Studies Hybridoma Bank for fly stocks and antibodies. We thank the following individuals for fly stocks, reagents, antibodies, and immunostaining protocols: Dr. Lucas Waltzer, Dr. Michele Crozatier, Dr. Elizabeth Rideout, Dr. Istvan Ando, Dr. Pauline Spéder, Dr. Mihaela Serpe, Dr. Thomas Kornberg, Dr. Pascal Thérond, Dr. Julie Simpson, and Dr. Isabel Guerrero. Funding for this study was provided by the grant to G.T. from Canadian Institutes of Health Research (Project Grant PJT-156277). K.Y.L.H. was supported by a Four-Year Doctoral Fellowship from University of British Columbia.

1. F. Ferraro, C. L. Celso, D. Scadden, Adult stem cels and their niches. *Adv. Exp. Med. Biol.* **695**, 155–168 (2010).
2. J. A. Martinez-Agosto, H. K. Mikkola, V. Hartenstein, U. Banerjee, The hematopoietic stem cell and its niche: A comparative view. *Genes Dev.* **21**, 3044–3060 (2007).
3. S. J. Morrison, A. C. Spradling, Stem cells and niches: Mechanisms that promote stem cell maintenance throughout life. *Cell* **132**, 598–611 (2008).
4. P. Rojas-Rios, A. Gonzalez-Reyes, Concise review: The plasticity of stem cell niches: A general property behind tissue homeostasis and repair. *Stem Cells* **32**, 852–859 (2014).
5. C. A. Chacon-Martinez, J. Koester, S. A. Wickstrom, Signaling in the stem cell niche: Regulating cell fate, function and plasticity. *Development* **145**, dev165399 (2018).
6. K. Kurokawa, Y. Hayakawa, K. Koike, Plasticity of intestinal epithelium: Stem cell niches and regulatory signals. *Int. J. Mol. Sci.* **22**, 357 (2020).
7. M. Boulet *et al.*, Characterization of the Drosophila adult hematopoietic system reveals a rare cell population with differentiation and proliferation potential. *Front. Cell Dev. Biol.* **9**, 739357 (2021).
8. I. Morin-Poulard, Y. Tian, N. Vanzo, M. Crozatier, Drosophila as a model to study cellular communication between the hematopoietic niche and blood progenitors under homeostatic conditions and in response to an immune stress. *Front. Immunol.* **12**, 719349 (2021).
9. F. Luo, S. Yu, L. H. Jin, The posterior signaling center is an important microenvironment for homeostasis of the Drosophila lymph gland. *Front. Cell Dev. Biol.* **8**, 382 (2020).
10. U. Banerjee, J. R. Girard, L. M. Goins, C. M. Spratford, Drosophila as a genetic model for hematopoiesis. *Genetics* **211**, 367–417 (2019).
11. S. H. Jung, C. J. Evans, C. Uemura, U. Banerjee, The Drosophila lymph gland as a developmental model of hematopoiesis. *Development* **132**, 2521–2533 (2005).
12. J. Krzemien *et al.*, Control of blood cell homeostasis in Drosophila larvae by the posterior signalling centre. *Nature* **446**, 325–328 (2007).
13. K. Y. L. Ho, R. J. Khadilkar, R. L. Carr, G. Tanentzapf, A gap-junction-mediated, calcium-signaling network controls blood progenitor fate decisions in hematopoiesis. *Curr. Biol. CB* **31**, 4697–4712. e4696 (2021).
14. B. Cho *et al.*, Single-cell transcriptome maps of myeloid blood cell lineages in Drosophila. *Nat. Commun.* **11**, 4483 (2020).
15. L. Mandal, J. A. Martinez-Agosto, C. J. Evans, V. Hartenstein, U. Banerjee, A Hedgehog- and Antennapedia-dependent niche maintains Drosophila haematopoietic precursors. *Nature* **446**, 320–324 (2007).
16. B. Benmimoun, C. Polesello, M. Haenlin, L. Waltzer, The EBF transcription factor Collier directly promotes Drosophila blood cell progenitor maintenance independently of the niche. *Proc. Natl. Acad. Sci. U.S.A.* **112**, 9052–9057 (2015).
17. T. Lebestky, S. H. Jung, U. Banerjee, A Serrate-expressing signaling center controls Drosophila hematopoiesis. *Genes Dev.* **17**, 348–353 (2003).
18. D. Pennetier *et al.*, Size control of the Drosophila hematopoietic niche by bone morphogenetic protein signaling reveals parallels with mammals. *Proc. Natl. Acad. Sci. U.S.A.* **109**, 3389–3394 (2012).
19. S. A. Sinenko, L. Mandal, J. A. Martinez-Agosto, U. Banerjee, Dual role of wingless signaling in stem-like hematopoietic precursor maintenance in Drosophila. *Dev. Cell* **16**, 756–763 (2009).
20. Y. Tokusumi, T. Tokusumi, D. A. Shoue, R. A. Schulz, Gene regulatory networks controlling hematopoietic progenitor niche cell production and differentiation in the Drosophila lymph gland. *PloS One* **7**, e41604 (2012).
21. I. Morin-Poulard *et al.*, Vascular control of the Drosophila haematopoietic microenvironment by Slit/Robo signalling. *Nat. Commun.* **7**, 11634 (2016).
22. B. Benmimoun, C. Polesello, L. Waltzer, M. Haenlin, Dual role for Insulin/TOR signaling in the control of hematopoietic progenitor maintenance in Drosophila. *Development* **139**, 1713–1717 (2012).
23. T. Tokusumi, Y. Tokusumi, D. W. Hopkins, R. A. Schulz, Bag of Marbles controls the size and organization of the Drosophila hematopoietic niche through interactions with the Insulin-like growth factor pathway and Retinoblastoma-family protein. *Development* **142**, 2261–2267 (2015).
24. V. Lam, T. Tokusumi, Y. Tokusumi, R. A. Schulz, bantam miRNA is important for Drosophila blood cell homeostasis and a regulator of proliferation in the hematopoietic progenitor niche. *Biochem. Biophys. Res. Commun.* **453**, 467–472 (2014).
25. R. J. Khadilkar *et al.*, ARF1-GTP regulates Asrij to provide endocytic control of Drosophila blood cell homeostasis. *Proc. Natl. Acad. Sci. U.S.A.* **111**, 4898–4903 (2014).
26. R. J. Khadilkar, W. Vogl, K. Goodwin, G. Tanentzapf, Modulation of occluding junctions alters the hematopoietic niche to trigger immune activation. *eLife* **6**, e28081 (2017).
27. A. A. Kim *et al.*, Independently paced Ca2+ oscillations in progenitor and differentiated cells in an ex vivo epithelial organ. *J. Cell Sci.* **135**, jcs260249 (2022).
28. P. Speder, A. H. Brand, Gap junction proteins in the blood-brain barrier control nutrient-dependent reactivation of Drosophila neural stem cells. *Dev. cell* **30**, 309–321 (2014).
29. D. A. Goodenough, D. L. Paul, Gap junctions. *Cold Spring Harb. Perspect. Biol.* **1**, a002576 (2009).
30. J. C. Herve, M. Derangeon, Gap-junction-mediated cell-to-cell communication. *Cell Tissue Res.* **352**, 21–31 (2013).
31. R. Bauer *et al.*, Intercellular communication: The Drosophila innexin multiprotein family of gap junction proteins. *Chem. Biol.* **12**, 515–526 (2005).
32. P. Phelan, Innexins: Members of an evolutionarily conserved family of gap-junction proteins. *Biochim. Biophys. Acta* **1711**, 225–245 (2005).
33. C. Lehmann *et al.*, Heteromerization of innexin gap junction proteins regulates epithelial tissue organization in Drosophila. *Mol. Biol. Cell* **17**, 1676–1685 (2006).
34. J. Guiza, I. Barria, J. C. Saez, J. L. Vega, Innexins: Expression, regulation, and functions. *Front. Physiol.* **9**, 1414 (2018).
35. J. Shim *et al.*, Olfactory control of blood progenitor maintenance. *Cell* **155**, 1141–1153 (2013).
36. T. Chorna, G. Hasan, The genetics of calcium signaling in Drosophila melanogaster. *Biochim. Biophys. Acta* **1820**, 1269–1282 (2012).
37. P. S. Chard, D. Bleakman, S. Christakos, C. S. Fullmer, R. J. Miller, Calcium buffering properties of calbindin D28k and parvalbumin in rat sensory neurones. *J. Physiol.* **472**, 341–357 (1993).
38. T. He, M. N. Nitabach, G. A. Lnenicka, Parvalbumin expression affects synaptic development and physiology at the Drosophila larval NMJ. *J. Neurogenetics* **32**, 209–220 (2018).
39. X. Xu, M. B. Bhat, M. Nishi, H. Takeshima, J. Ma, Molecular cloning of cDNA encoding a drosophila ryanodine receptor and functional studies of the carboxyl-terminal calcium release channel. *Biophys. J.* **78**, 1270–1281 (2000).
40. H. Deng, A. A. Gerencser, H. Jasper, Signal integration by Ca(2+) regulates intestinal stem-cell activity. *Nature* **528**, 212–217 (2015).
41. D. De Stefani, M. Patron, R. Rizzuto, Structure and function of the mitochondrial calcium uniporter complex. *Biochim. Biophys. Acta* **1853**, 2006–2011 (2015).
42. S. Choi *et al.*, Mitochondrial calcium uniporter in Drosophila transfers calcium between the endoplasmic reticulum and mitochondria in oxidative stress-induced cell death. *J. Biol. Chem.* **292**, 14473–14485 (2017).
43. K. Thurley *et al.*, Reliable encoding of stimulus intensities within random sequences of intracellular Ca2+ spikes. *Sci. Signal.* **7**, ra59 (2014).
44. K. Masuyama, Y. Zhang, Y. Rao, J. W. Wang, Mapping neural circuits with activity-dependent nuclear import of a transcription factor. *J. Neurogenetics* **26**, 89–102 (2012).
45. A. Skupin *et al.*, How does intracellular Ca2+ oscillate: By chance or by the clock? *Biophys. J.* **94**, 2404–2411 (2008).
46. E. Smedler, S. Malmersjo, P. Uhlen, Network analysis of time-lapse microscopy recordings. *Front. Neural Circ.* **8**, 111 (2014).
47. A. L. Barabasi, Z. N. Oltvai, Network biology: Understanding the cell's functional organization. *Nat. Rev. Genet.* **5**, 101–113 (2004).
48. M. Rubinov, O. Sporns, Complex network measures of brain connectivity: Uses and interpretations. *NeuroImage* **52**, 1059–1069 (2010).
49. L. Leybaert, M. J. Sanderson, Intercellular Ca(2+) waves: Mechanisms and function. *Physiol. Rev.* **92**, 1359–1392 (2012).
50. A. J. Laude, A. W. Simpson, Compartmentalized signalling: Ca2+ compartments, microdomains and the many facets of Ca2+ signalling. *FEBS J.* **276**, 1800–1816 (2009).
51. J. A. Orellana, H. A. Sanchez, K. A. Schalper, V. Figueroa, J. C. Saez, Regulation of intercellular calcium signaling through calcium interactions with connexin-based channels. *Adv. Exp. Med. Biol.* **740**, 777–794 (2012).
52. A. Skupin, K. Thurley, Calcium signaling: From single channels to pathways. *Adv. Exp. Med. Biol.* **740**, 531–551 (2012).
53. M. Vignes, E. Blanc, I. Sassetti, M. Recasens, Intra- vs extracellular calcium regulation of neurotransmitter-stimulated phosphoinositide breakdown. *Neurochem. Int.* **28**, 145–153 (1996).
54. S. Malmersjo *et al.*, Neural progenitors organize in small-world networks to promote cell proliferation. *Proc. Natl. Acad. Sci. U.S.A.* **110**, E1524–1532 (2013).
55. A. Ravella, T. Ringstedt, J. P. Brion, M. Pandolfo, E. Herlenius, Adult neural precursor cells form connexin-dependent networks that improve their survival. *Neuroreport* **26**, 928–936 (2015).
56. Y. Fujii, S. Maekawa, M. Morita, Astrocyte calcium waves propagate proximally by gap junction and distally by extracellular diffusion of ATP released from volume-regulated anion channels. *Sci. Rep.* **7**, 13115 (2017).
57. D. Segretain, M. M. Falk, Regulation of connexin biosynthesis, assembly, gap junction formation, and removal. *Biochim. Biophys. Acta* **1662**, 3–21 (2004).
58. M. Crozatier, A. Vincent, Control of multidendritic neuron differentiation in Drosophila: The role of Collier. *Dev. Biol.* **315**, 232–242 (2008).
59. J. H. Simpson, Rationally subdividing the fly nervous system with versatile expression reagents. *J. Neurogenetics* **30**, 185–194 (2016).
60. P. A. Brodskiy, J. J. Zartman, Calcium as a signal integrator in developing epithelial tissues. *Phys. Biol.* **15**, 051001 (2018).
61. J. E. Purvis, G. Lahav, Encoding and decoding cellular information through signaling dynamics. *Cell* **152**, 945–956 (2013).
62. P. A. Brodskiy *et al.*, Decoding calcium signaling dynamics during Drosophila wing disc development. *Biophys. J.* **116**, 725–740 (2019).
63. Y. Tokusumi, T. Tokusumi, J. Stoller-Conrad, R. A. Schulz, Serpent, suppressor of hairless and U-shaped are crucial regulators of hedgehog niche expression and prohemocyte maintenance during Drosophila larval hematopoiesis. *Development* **137**, 3561–3568 (2010).
64. P. De Koninck, H. Schulman, Sensitivity of CaM kinase II to the frequency of Ca2+ oscillations. *Science* **279**, 227–230 (1998).
65. R. Petrova, A. L. Joyner, Roles for Hedgehog signaling in adult organ homeostasis and repair. *Development* **141**, 3445–3457 (2014).
66. J. Oyallon *et al.*, Two independent functions of Collier/Early B cell factor in the control of Drosophila blood cell homeostasis. *PloS one* **11**, e0148978 (2016).
67. M. Destalminil-Letourneau, I. Morin-Poulard, Y. Tian, N. Vanzo, M. Crozatier, The vascular niche controls Drosophila hematopoiesis via fibroblast growth factor signaling. *eLife* **10**, e64672 (2021).